The rare sugar *N*-acetylated viosamine is a major component of Mimivirus fibers

Received for publication, February 27, 2017, and in revised form, March 16, 2017 Published, Papers in Press, March 17, 2017, DOI 10.1074/jbc.M117.783217

Francesco Piacente[‡], Cristina De Castro[§], Sandra Jeudy[¶], Matteo Gaglianone[‡], Maria Elena Laugieri[‡], Anna Notaro[¶‖1], Annalisa Salis[‡], Gianluca Damonte[‡], Chantal Abergel[¶], and Michela G. Tonetti[‡2]

From the [‡]Department of Experimental Medicine and Center of Excellence for Biomedical Research, University of Genova, 16126 Genova, Italy, the Departments of [§]Agricultural Sciences and [‖]Chemical Sciences, University of Napoli, 80138 Napoli, Italy, and the [¶]Aix-Marseille Université, Centre National de la Recherche Scientifique, Information Génomique et Structurale, UMR 7256, IMM FR3479, 13288 Marseille Cedex 9, France

Edited by Gerald W. Hart

The giant virus Mimivirus encodes an autonomous glycosylation system that is thought to be responsible for the formation of complex and unusual glycans composing the fibers surrounding its icosahedral capsid, including the dideoxyhexose viosamine. Previous studies have identified a gene cluster in the virus genome, encoding enzymes involved in nucleotide-sugar production and glycan formation, but the functional characterization of these enzymes and the full identification of the glycans found in viral fibers remain incomplete. Because viosamine is typically found in acylated forms, we suspected that one of the genes might encode an acyltransferase, providing directions to our functional annotations. Bioinformatic analyses indicated that the L142 protein contains an N-terminal acyltransferase domain and a predicted C-terminal glycosyltransferase. Sequence analysis of the structural model of the L142 N-terminal domain indicated significant homology with some characterized sugar acetyltransferases that modify the C-4 amino group in the bacillosamine or perosamine biosynthetic pathways. Using mass spectrometry and NMR analyses, we confirmed that the L142 N-terminal domain is a sugar acetyltransferase, catalyzing the transfer of an acetyl moiety from acetyl-CoA to the C-4 amino group of UDP-D-viosamine. The presence of acetylated viosamine *in vivo* has also been confirmed on the glycosylated viral fibers, using GC-MS and NMR. This study represents the first report of a virally encoded sugar acetyltransferase.

Previous reports have provided evidence that the genome of some giant and large DNA viruses encodes autonomous glycosylation systems (1, 2). These machineries include glycosyltransferases and the enzymes required to produce their nucleotide-sugar substrates. Interestingly, for the few cases reported so far (3–5), novel and atypical glycans have been described. Pathways for monosaccharide synthesis and complex glycan structures have been characterized in *Chlorella* viruses (Phycodnaviridae family) and in some members of the Mimiviridae family (6–11). In this frame, analysis of the genomes of newly identified giant viruses suggests that *Chlorella* viruses and Mimiviridae are not isolated cases, because genes associated with glycosylation pathways are found in other members of the nucleocytoplasmic large DNA viruses (12).

Mimivirus is the first identified member of the growing family of Mimiviridae (13). Its 1.2-Mbp genome encodes ~1000 proteins, and the pseudoicosahedral virions of 400-nm diameter are covered by a dense array of 150-nm-long, highly glycosylated fibers (14). The micrometer size of the viral particles together with the glycosylated fibers mimics the bacteria on which the Mimivirus natural host, *Acanthamoeba castellanii*, feeds. In a previous study, data from compositional analysis of Mimivirus glycans preparations revealed the presence of various monosaccharides, including *N*-acetylglucosamine, glucose, rhamnose, and the very rare 4-amino-4,6-dideoxyhexose viosamine along with its methylated derivative (6). The genes encoding the putative enzymes of the UDP-D-viosamine biosynthesis pathway have been identified in a 9-gene cluster localized at the 5′ end of Mimivirus genome, possibly devoted to glycan production (6). Specifically, the first enzyme, R141, is an UDP-D-glucose 4,6-dehydratase that catalyzes the formation of a UDP-4-keto-6-deoxy intermediate, also common to the UDP-L-rhamnose pathway (8). A pyridoxal phosphate-dependent aminotransferase, L136, then transfers an amino group from glutamate to the 4-keto group, leading to UDP-D-Vio[3] production (6).

Viosamine has only been identified in some bacterial species. In *Pseudomonas syringae* it is a component of the flagellin-associated trisaccharide required for virulence, and in this case the 4-amino group is acylated, and a 2-*O*-methyl group is also present (15, 16). This unusual sugar, 2-*O*-methyl-4-(3-hydroxy-3-methylbutanamido)-4,6-dideoxy-D-glucose, is also termed anthrose, because of its occurrence in *Bacillus anthra-*

This work was supported in part by the Fondo per la Ricerca di Ateneo, University of Genova, and French National Research Agency Grant ANR-14-CE14-0023-01. The authors declare that they have no conflicts of interest with the contents of this article.

[1] Recipient of a UIF Vinci program 2015 Ph.D. Fellowship C3_90.

[2] To whom correspondence should be addressed: Dept. of Experimental Medicine, University of Genova, Viale Benedetto XV, 1-16132 Genova, Italy. Tel.: 39-010-3538151; Fax: 39-010-35338162; E-mail: tonetti@unige.it.

[3] The abbreviations used are: Vio, viosamine; VioNAc, *N*-acetylviosamine; ESI, electrospray ionization; HSQC, heteronuclear single-quantum correlation spectroscopy; HMBC, heteronuclear multiple-bond correlation spectroscopy; PMAA, partially methylated alditol acetate; LβH, left-handed β-helix; GT, glycosyltransferase; N-L142, N-terminal domain of L142; TOCSY, total correlation spectroscopy; CPK, Corey-Pauling-Koltun.

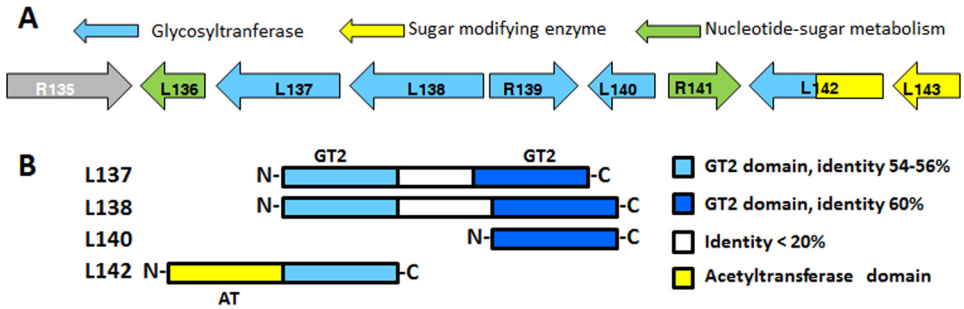

Figure 1. Organization of the L142 gene cluster. *A*, in addition to L142, the 9-gene cluster contains the two enzymes for UDP-D-Vio production (R141 and L136), a putative pyruvoyltransferase (L143), a structural protein of the outer fibers (R135), and putative glycosyltransferases (L137, L138, R139, and L140). *B*, organization of the glycosyltransferase domains. *AT*, acetyltransferase domain; *GT2*, glycosyltransferase domain.

cis exosporium (17). Modified Vio has also been reported in few other bacterial organisms (18–25).

Because Vio is always acylated on the amino group, we undertook a study to verify its status in Mimivirus by adopting a dual strategy. First, we scrutinized the cluster in search of a candidate for Vio acetylation and identified the N-terminal domain of L142 protein as a possible acyltransferase. Second, we performed GC-MS and NMR analyses of Mimivirus glycans. We now report the characterization of the N-terminal domain of L142 (N-L142) as an acetyl-CoA-dependent enzyme able to modify the 4-amino group of UDP-D-Vio. GC-MS and NMR analyses of Mimivirus glycans then confirmed that Vio is completely acetylated *in vivo*. To our knowledge, this represents the first report of a virally encoded sugar-*N*-acetyltransferase.

Results

Sequence and structure analysis

L142 gene product is a bifunctional protein with an N-terminal domain with a predicted left-handed β-helix (LβH) superfamily fold and a C-terminal one, predicted as glycosyltransferase because of sequence homology. L142 is part of the 9-gene cluster (6) encoding two enzymes involved in UDP-D-Vio production (L136 and R141), the R135 protein already identified as a component of the outer fibers (26, 27) and several putative glycosyltransferases, some of them displaying two domains possibly derived from gene duplication events, as shown in Fig. 1. In particular, the C-terminal domain of L142 has strong homology with the N-terminal regions of L137 and L138 (Fig. 1), both predicted to be type 2 glycosyltransferases (GT-2) (26). The C-terminal domain of L142 is also predicted to belong to GT-2 family in the CAZy database (28).

Bioinformatic analysis of the N-L142 revealed the presence of a hexapeptide repeat motif, typical of the LβH domain, initially described in UDP-*N*-acetylglucosamine 3-*O*-acyltransferase (LpxA) (29). The LβH domain is found in many acyltransferases and contributes to the subunit interface, promoting trimerization, as well as active site formation. As already observed for L136, the enzyme that transfers the C-4 amino group, no close homologue of N-L142 was found in other viral genomes, excluding Mimivirus close relatives. In the Mimiviridae family, BLAST best hits corresponded to uncharacterized proteins from different bacterial species (with 30–37% identity over 196 amino acids) and from environmental sequences. The sequence conservation of N-L142 with known sugar acetyltransferases is reported in Table 1.

Interestingly, N-L142 did not show homology with enzymes known to modify Vio, such as VioB and AntD (15, 22, 30). Low homology was found with QdtC, which modifies the 3-amino group in the synthesis of dTDP-3-acetamido-3,6-dideoxy-α-D-glucose (31). On the other hand, a significant homology was observed with the well-characterized PglD from *Campylobacter jejuni*, as well as with the C-terminal ATD domains of *Neisseria gonorrhoeae* PglB and *Acinetobacter baumannii* WeeI, all catalyzing an acetyl transfer to the C-4 amino group for UDP-D-BacNAc$_2$ (32, 33). Among the characterized sugar acetyltransferases, the best hit was with *Caulobacter crescentus* PerB catalyzing the last step of GDP-D-*N*-acetyl-perosamine synthesis (34). The structural alignment of N-L142 with PglD, PglB, WeeI, and PerB is reported in Fig. 2, which also highlights the residues involved in catalysis and substrate recognition (32–34).

Structural comparison of the N-L142 Phyre2 model with *N. gonorrhoeae* PglB confirmed that it possesses all the necessary determinants for acetyl-CoA and UDP-D-Vio recognition, as well as the catalytic residues involved in acetyl transfer and those involved in trimer formation. Interestingly, the structural comparison of the N-L142 model (Fig. 3), based on PglB (4M99), with the PerB (4EA8) structure in complex with acetyl-CoA and GDP-D-*N*-acetylperosamine highlighted a steric hindrance caused by an aspartate residue (Asp-232 in 4M99, Asp-40 in L142, and Asp-39 in 4EA8) in the nucleotide-binding site, preventing the accommodation of GDP but allowing a UDP to be properly positioned in the cavity. Asp-55 in PerB is also replaced by Thr-247 in PglB and Ile-55 in N-L142. The overall loop is in a closer state than in the GDP bound structure. Moreover, whereas in the PglB structure an asparagine residue is known to interact with the acetyl bound to the C-2 amino group in bacillosamine (Asn-162), in the N-L142 model, it is another strand of the LβH that provides a specific residue (Arg-155), able to engage a H-bond with the hydroxyl group in C-2 of the viosamine. This suggests that viosamine methylation in C-2 is the last step of the sugar modification, probably after the transfer of VioNAc on its acceptor.

Purification of recombinant N-L142 and enzymatic activity

WT N-142 and H136A and H145A mutants, expressed as GST-fusion proteins, were purified to homogeneity using affinity purification. WT and mutant proteins were soluble after proteolytic release from GST; comparable amounts, 2–4 mg/li-

Table 1
Sequence identity of N-L142 with characterized sugar acetyltransferases

	Protein	Product	Reference	Identity
				%
BAH58344	VioB *P. syringae*	dTDP-D-VioNAc	Ref. 15	18
Q9XCW3	VioB *E. coli*	dTDP-D-VioNAc	Ref. 22	
3VBJ_A	AntD *Bacillus cereus*	dTDP-D-anthrose	Ref. 29	
AAR85517	QdtC *Thermoanaerobacterium thermosaccharolyticum*	dTDP-3-acetamido-3,6-dideoxy-D-glucose (30)	Ref. 30	25
4M99	PglB *N. gonorrhoeae*	UDP-D-BacNAc$_2$	Ref. 31	30
3BSS	PglD *C. jejuni*	UDP-D-BacNAc$_2$	Ref. 32	30
4M9C	WeeI *A. baumannii*	UDP-D-BacNAc$_2$	Ref. 32	24
4EA8	PerB *C. crescentus*	GDP-D-*N*-acetyl-perosamine	Ref. 33	32

```
N-L142      --MSITSVS---LYVYLICAGGHAKQVIDIFLDNG----IEI-KGIFDDNKTGQFYRGTQIIG
PglB        --MA------GNRKLAVIGAGGHGKVVAELAAALG----TYGEIVFLDD-RTQGSVNGFPVIG
PerB        GHMGAASASLAIGGVVIIGGGGHAKVVIESLRACG----ETV-AAIVDADPTRRAVLGVPVVG
WeeI        -------MT---MIIGVYGASGFGKEVMPLVRQQFPTLSKEQ-FAFIDDGLSGTTLNGYPVLS
PglD        --GSAMART---EKIYIYGASGHGLVCEDVAKNMG----YKE-CIFLDDFKGMKF--------

N-L142      VISD---ITKYQSEPFFCTVGDNQIREKISQTVGN--VEWINCISKLAYISPSVVIG--KGNY
PglB        TTLLLENSLSPEQFDITVAVGNNRIRRQITENAAALGFKLPVLIHPDATVSPSAIIG--QGSV
PerB        DDLALPMLREQGLSRLFVAIGDNRLRQKLGRKARDHGFSLVNAIHPSAVVSPSVRLG--EGVA
WeeI        YLDF--ISKPADHKAVTIAIANSVVREKLVSLLEKDGVQHLAVQSTNTVILDEVEIG--EGSL
PglD        -------ESTLPKYDFFIAIGNNEIRKKIYQKISENGFKIVNLIHKSALISPSAIVEENAGIL

                                          *                 *
N-L142      VGTHSKILADSQLGDFNIVNEGATLTHDNIIGDFNHIAPNVSVGGRVKIGNFNLIGTNSTVNP
PglB        VMAKAVVQAGSVLKDGVIVNTAATVDHDCLLDAFVHISPGAHLSGNTRIGEESRIGTGACSRQ
PerB        VMAGVAINADSWIGDLAIINTGAVVDHDCRLGAACHLGPASALAGGVSVGERAFLGVGARVIP
WeeI        LCPFTCLTSNIKIGKFFHANIYSYVAHDCVIGDYVTFAPGAKCNGNIHIEDHAYIGTGAVIKQ
PglD        IMPYVVINAKAKIEKGVILNTSSVIEHECVIGEFSHVSVGAKCAGNVKIGKNCFLGINSCVLP

N-L142      -----DILISNNIIIGSGATVVKSLVDPGIYIGTPCKKIIKNISDK
PglB        -----QTTVGSGVTAGAGAVIVCDIPDGMTVAGNPAKPL-------
PerB        -----GVTIGADTIVGAGGVVVRDLPDSVLAIGVPAKIKGDRS---
WeeI        GTPDKPLIIGKGAIVGMGAVVTKSVPAGVTVVGNPARILERK----
PglD        -----NLSLADDSILGGGATLVKNQDEKGVFVGVPAKRM-------
                  *
```

Figure 2. Structural alignment of N-L142. Shown are the C-terminal ATD domains of *N. gonorrhoeae* PglB (4M99), *C. crescentus* PerB (4EA8), *A. baumannii* WeeI (4M9C), and *C. jejuni* PglD (3BSS). Residues involved in trimer interface and in acetyl-coA binding site are marked in *red* (based on cd03360, Ref. 43, and our analyses of the model). The conserved catalytic histidine is marked by a *blue star*, and the position corresponding to viosamine C-2-O binding in L142 is marked by a *red star* (Arg-155 in *bold*), whereas the PglD Asn-162 residue involved in C-2 acetylbacillosamine binding is marked by a *green star*.

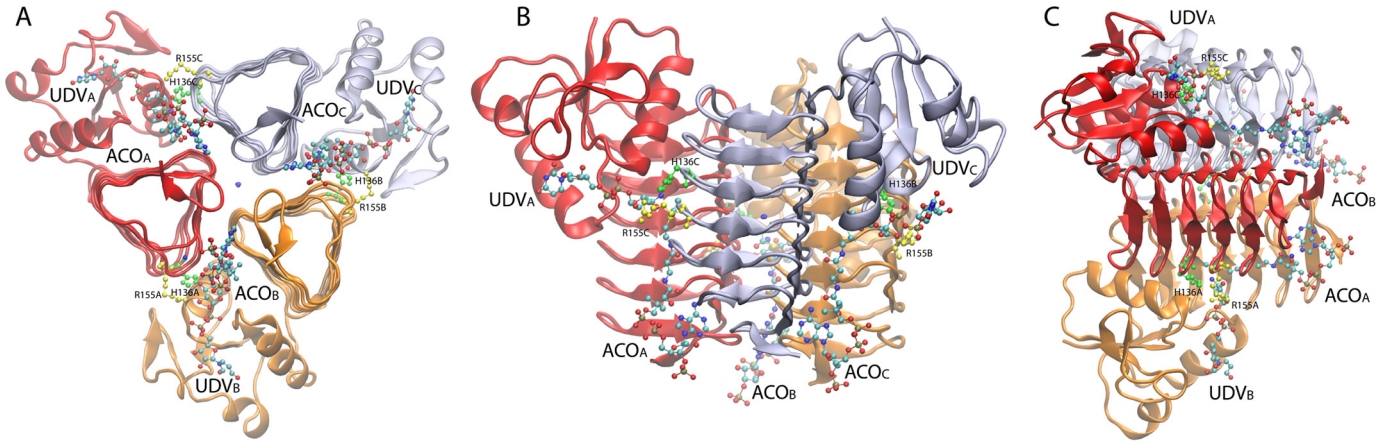

Figure 3. Ribbon representation of three perpendicular orientations (*A*, *B*, and *C*) of the N-L142 homotrimer model. Each monomer has a different color for clarity (chain A in *red*, chain B in *orange*, chain C in *ice blue*). *Panel B* corresponds to a 90° rotation of the A orientation around the horizontal axis and C to a 90° rotation around the vertical axis. The acetyl-CoA (*ACO*) and UDP-D-*N*-acetylviosamine (*UDV*) are represented as CPKs colored by atom types. The Arg-155 residue making H-bonds with the viosamine C-2O in each monomer is represented as *yellow* CPK, and the catalytic His-136 is represented as *green* CPK. The figure was produced using VMD - Visual Molecular Dynamics.

ter of bacterial culture, were obtained for WT and mutant proteins.

UDP-D-Vio was produced as described (6) and used as substrate in the enzymatic activity assays. UDP-D-Vio (Fig. 4, *peak A*) was incubated with purified WT N-L142 and acetyl-CoA; product formation was monitored by anion-exchange HPLC (Fig. 4, *peak B*). Enzymatic activity of H136A mutant incubated in identical condition resulted in a decrease by 3 orders of mag-

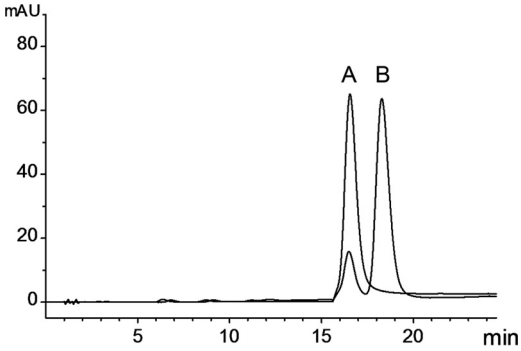

Figure 4. Anion-exchange HPLC analysis of nucleotide sugars. UDP-D-Vio (*peak A*) was incubated with the recombinant L142 N-terminal domain in the presence of acetyl-CoA at 25 °C. The progressive formation of a new compound (*peak B*) was observed.

nitude of the enzymatic activity (3992 ± 554 μmol/min/mg protein for the WT *versus* 2.1 ± 1.5 μmol/min/mg protein for the H136A mutant tested within 48 h from purification). In addition, the WT protein activity remained stable over a week of storage, whereas the H136A mutant displayed ~20–30% decrease. An increase in absorbance at 332 nm, suggestive of protein aggregation, or the presence of a precipitate were not observed for the WT or H136A proteins. Indeed, the reduced enzymatic activity found for this mutant is likely due to the role that His-136 has in the catalytic mechanism rather than to the perturbation of the protein fold. This conclusion is also in agreement with the proposed role of the active site His in the catalytic mechanism for the PglD and PerB enzymes (33). No significant changes in the enzymatic activity were observed for the H145A mutant, in agreement with previous reports for PglD and PerB, where mutation of the corresponding His caused only minor effects in the catalytic activity (33).

Structural characterization of L142 product

The L142 product was purified using anion-exchange HPLC and solid-phase extraction, as described (6), for further ESI-MS and NMR analyses. ESI-MS revealed the presence of a main ion at 590 *m*/*z*, consistent with the expected mass of UDP-D-VioNAc (Fig. 5). A minor peak of 611.9 *m*/*z*, was consistent with the sodium adduct of UDP-D-VioNAc.

The purified product was also analyzed by NMR. Identification of the UDP-D-VioNAc signals was possible by using both 2D homo- and heteronuclear NMR sequences (Table 1). The area at 6.0–5.5 ppm (Fig. 6*A*) contained H-5 of the uracil moiety and two anomeric signals; the one at 5.99 ppm belonged to the expected ribofuranose unit of the UDP. Our analysis focused on that second one, which had to be related to the Vio residue. The proton at 5.57 ppm correlated with a carbon at 96.5 ppm (HSQC spectrum in Fig. 6*B*), a chemical shift similar to that previously reported for the non *N*-acetylated form of UDP-D-Vio (6). Similarly to that, H-1 of *N*-acetyl-Vio appeared as a double doublet because of the coupling with two NMR active nuclei, phosphorous ($^3J_{H1,P}$ 6.7 Hz) and H-2 ($^3J_{H1,H2}$ 3.3 ppm). Identification of all the ring proton resonances was accomplished by COSY spectrum interpretation (Fig. 6*C*). H-2 was at 3.61 ppm, partially overlapped to H-4. Nevertheless it was possible to evaluate the multiplicity of both proton signals: H-2 was a double triplet (Fig. 6, inset) caused by the coupling to H-1 ($^3J_{H2,H1}$ 3.3 Hz), to phosphorous ($^4J_{H2,P}$ 3.3 Hz) and H-3 ($^3J_{H2,H3}$ 9.8 Hz). Both H-3 (3.76 ppm) and H-4 (3.62 ppm) appeared as triplet (^3J 10.0 Hz) meaning that, like H-2 and H-5, they were axial substituents of the pyranose ring of the sugar. This information confirmed the *gluco* stereochemistry of the sugar, whereas the carbon chemical shift of C-4 (57.6 ppm) together with H-6/C-6 (1.17/18.2 ppm) values confirmed that it was Vio. Importantly, compared with the non-acetylated Vio, H-4 was at lower field (3.62 *versus* 3.02 ppm), indicating that the amino function was acetylated, as confirmed by the occurrence of an acetyl group in the proton/carbon spectrum at $^1H/^{13}C$ 2.03/23.3 ppm, in a 1:1 ratio with the methyl group of the 6-deoxy position. The HMBC spectrum (Fig. 6*B*) disclosed that the methyl of this acetyl and H-4 correlated with the same carbonyl group (175.6 ppm), demonstrating that Vio was *N*-acetylated.

VioNAc from Mimivirus surface glycans

The sugar composition of Mimivirus glycans was already investigated by GC-MS in a previous study (6). After the alditol acetate derivatization, the major components of viral glycans were rhamnose, glucose, *N*-acetylglucosamine, and Vio. Analysis of the fragmentation spectrum of an unknown peak revealed the presence of methyl-Vio. However, the presence of acetylation on the C-4 amino group could not be detected using this method. Thus, Vio acylation on the surface of purified Mimivirus particles was analyzed by partially methylated alditol acetate (PMAA) method, followed by GC-MS analysis. The presence of a single peak containing one methyl group on Vio C-4 amino group, as evidenced by GC-MS fragmentation spectrum, is consistent with complete *N*-acylation of this monosaccharide in Mimivirus glycan (Fig. 7). In addition, PMAA analysis indicated that Vio is terminal and not further elongated by other sugars (Fig. 7).

The presence of Vio and the identity of the *N*-linked substituent were confirmed by NMR analyses (Fig. 8 and Table 1) of the glycans extracted from Mimivirus. Inspection of the HSQC spectrum (Fig. 8*C*) disclosed a complex pattern of anomeric signals (^1H range 5.1–4.5 ppm), a crowded carbinolic area (^1H range 4.4–3.1 ppm), two main acetyl signals (~ 2.0 ppm), and a group of methyl signals (not shown) characteristic of 6-deoxy-sugars at ~1.3 ppm. All these signals suffered of low resolution, and recording the spectra at high temperature did not improve their overall quality. However, identification of the Vio unit was achieved, even though it was not possible to determine at which residue it was further connected.

Vio anomeric signal was at ($^1H/^{13}C$) 4.59/105.3 ppm, values diagnostic of a residue β configured at the anomeric center. The TOCSY spectrum (Fig. 8*B*) disclosed that this signal correlated with other five protons (3.64, 3.56, 3.54, 3.22, and 1.24 ppm): this correlation pattern along with the presence of a methyl group at 1.24 ppm, identified this unit as Vio, labeled with *V*. Combination of COSY and TOCSY spectra established the sequence of the different protons, whereas HSQC identified the corresponding carbon chemical shifts (Table 2). H-2 (3.22 ppm) correlated with a carbon at low field (84.3 ppm) because it was methylated at the corresponding hydroxyl function (O-CH_3 at $^1H/^{13}C$ 3.63/60.9 ppm), as confirmed by the $V_{2,2OMe}$ and

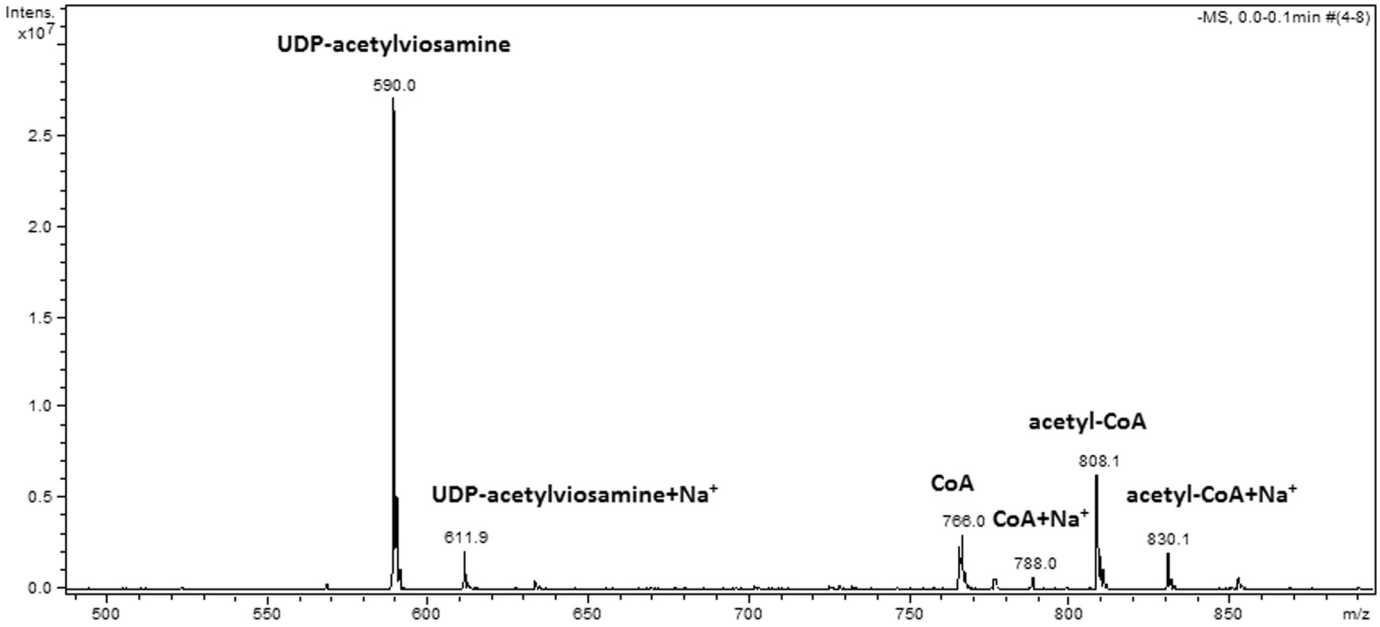

Figure 5. ESI-MS spectrum of the purified N-L142 product. The purified product of N-L142 was analyzed by ESI-MS. The main ion of 590 *m/z* corresponds to the calculated UDP-D-VioNAc molecular mass. Ion 612 *m/z* represents the sodium adduct. Other peaks are consistent with residual Acetyl-CoA and CoA-SH and their sodium adducts, copurified with the UDP-D-VioNAc.

$V_{2OMe,2}$ cross-peaks in the HMBC spectrum (Fig. 8*C*). H-2 enabled H-3 identification, which in turn led to H-4; H-5 was found almost coincident with H-3, as suggested from NOESY spectrum (Fig. 8*A*), which had one intense cross-peak at ~3.55 ppm embracing both H-3 and H-5; H-5 correlated further with H-6. Inspection of long-range correlations from H-6 (1.24 ppm) identified both C-4 and C-5 (57.8 and 72.0 ppm, respectively) so that C-3 value was finally selected and confirmed, and its value was indicated by the H-4/C-3 correlation in the HMBC spectrum (Fig. 8*C*). Of note, H-4 chemical shift (3.64 ppm) was similar to that of UDP-D-VioNAc (3.62 ppm) and not to that of UDP-D-Vio (3.02 ppm), in agreement with the amino function acylation. Accordingly, both H-4 and the methyl of the acetyl at 2.07 ppm had a long-range correlation with a carbonyl at 175.1 ppm, disclosing that the acyl of the amino group was an acetyl.

Indeed, in the polysaccharide fibers, Vio has a β-anomeric linkage, is methylated at position 2, is acetylated at the amino function, and has no other substituent; it occupies a terminal position in agreement with PMAA analysis. HMBC and NOESY spectra identified the density of a monosaccharide linked with Vio (see at the *cross* of the *dotted lines* in Fig. 8), but poor spectra resolution hampered the elucidation of the nature of this residue.

Discussion

Previous studies showed that the unusual sugar Vio is a component of Mimivirus glycans and that it is mainly contained in the long fibers that surround the capsid (5, 6). Here we demonstrate that the 4-amino group of UDP-D-Vio is acetylated by the N-terminal domain of the L142 gene product. The *in vitro* data obtained with the recombinant enzyme are consistent with the finding that Vio is also *N*-acetylated *in vivo* in Mimivirus glycans. Indeed, GC-MS and NMR data clearly indicate that, in fibers, Vio is terminal and is both *N*-acetylated on C-4 and methylated on C-2.

Viosamine, acetylated on the C-4 amino group and often also methylated on C-2, is restricted to some bacterial species, pathogenic to both vertebrates and plants. In *P. syringae*, dTDP-VioNAc is produced by a set of enzymes contained in a gene cluster named "Vio island," which includes VioA, which transfers the amino group to the 4-keto group of dTDP-4-keto-6-deoxy-D-glucose and VioB that acetylates the 4-amino group (15). Other enzymes in the cluster further convert dTDP-D-VioNAc to dTDP-D-*N*-(3-hydroxy-1-oxobutyl)Vio and its 2-methylated derivative. Modified Vio was found in the flagellin-associated glycans, and disruption of its biosynthetic pathway impairs motility and virulence on host tobacco leaves (16). Similar "Vio islands" were also identified in *P. aeruginosa* PAK (15, 35) and in *B. anthracis* (17). In this latter organism, modified Vio is a component of the exosporium pentasaccharide (17, 29). The biosynthetic genes for dTDP-VioNAc were also identified in *Escherichia coli* O7 and *Shigella dysenteriae* type 7 (22). However, in most cases the acetyl group is further modified into more complex moieties, and simple acetylation has been rarely reported.

Bioinformatic analysis of N-L142 sequence showed that, surprisingly, it has no homology to known enzymes involved in Vio *N*-acetylation or acylation. Similarly, the first enzyme of the Mimivirus Vio pathway, L136, has very low homology with the corresponding VioA of *P. syringae* or *E. coli*. On the other hand, a significant homology was found with enzymes that catalyze the acetylation of the 4-amino group of UDP-D-BacNAc (31, 33). $BacNAc_2$ is an essential component of bacterial *N*-linked and *O*-linked glycans, where it represents the first sugar attached to the protein. Moreover, good homology was found with *C. crescentus* PerB, responsible for GDP-D-perosamine acetylation (34). This finding was also confirmed by comparison of N-L142 structural model with *N. gonorrhoeae* PglB and *C. crescentus* PerB (Fig. 3). N-L142 shows a typical LβH super-

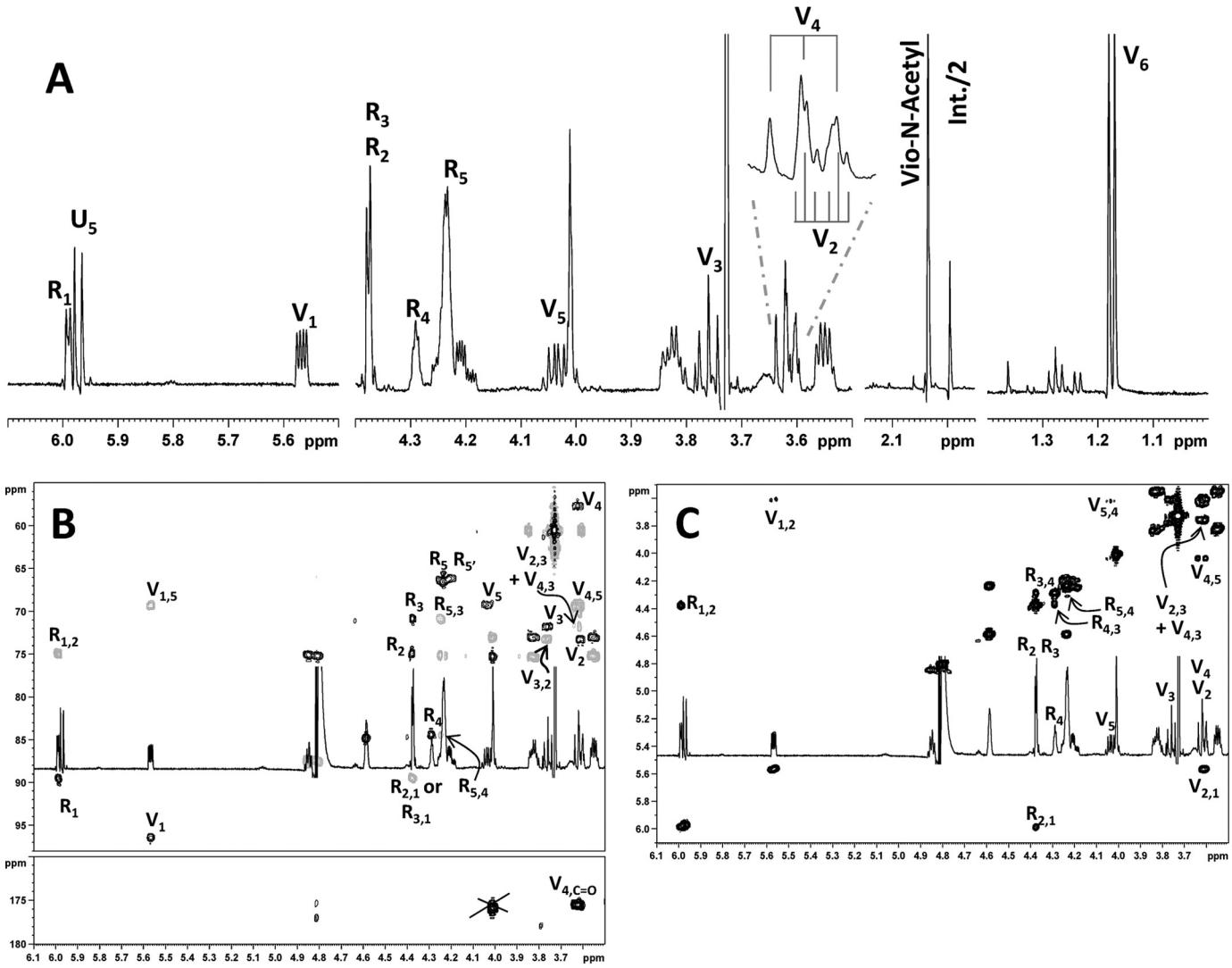

Figure 6. NMR analysis of purified UDP-D-VioNAc. *A*, full proton spectrum recorded for UDP-D-VioNAc (600 MHz, 25 °C, D_2O). The *inset* details H-2 and H-4 signals, and the *gray dotted lines* dissect the contribution given by each proton to the complex signal. Only signals belonging to ribose (*R*) and Vio (*V*) are labeled; other signals belong to residual NADPH or impurities. *B*, expansion of COSY spectrum of UDP-D-VioNAc (600 MHz, 25 °C, D_2O). Only densities belonging to ribose (*R*) and viosamine (*V*) cross-peak densities are attributed; other signals belong to residual NADPH or impurities. *C*, expansion of COSY spectrum of UDP-D-VioNAc (600 MHz, 25 °C, D_2O). Only cross-peak densities belonging to ribose (*R*) and viosamine (*V*) are attributed; other signals belong to residual NADPH.

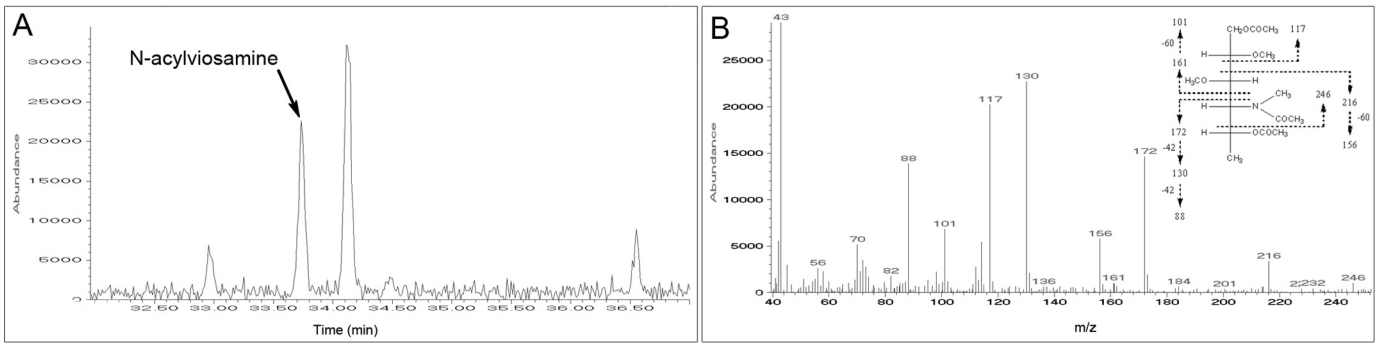

Figure 7. Identification of *N*-acylated Vio in Mimivirus by PMAA GC-MS analysis. The viral particles were derivatized by PMAA technique and then analyzed by GC-MS. The chromatogram of VioNAc was obtained by extraction of *m/z* 117 ion current. Peak identification was performed by comparing UDP-D-VioNAc standard analysis and fragmentation spectra. *A*, zoomed-in view of the *m/z* 117 extracted chromatogram of Mimivirus. *B*, fragmentation spectrum of VioNAc

family fold, typical of this type of acyltransferases. Chantigian *et al.* (36), starting from X-ray structures and site-directed mutagenesis analyses, have proposed the presence of two different classes of LβH enzymes able to acylate nucleotide sugars, based on substrate binding orientations and reaction mechanisms. *N. gonorrhoeae* PglB, *C. jejuni* PglD, and *C. crescentus*

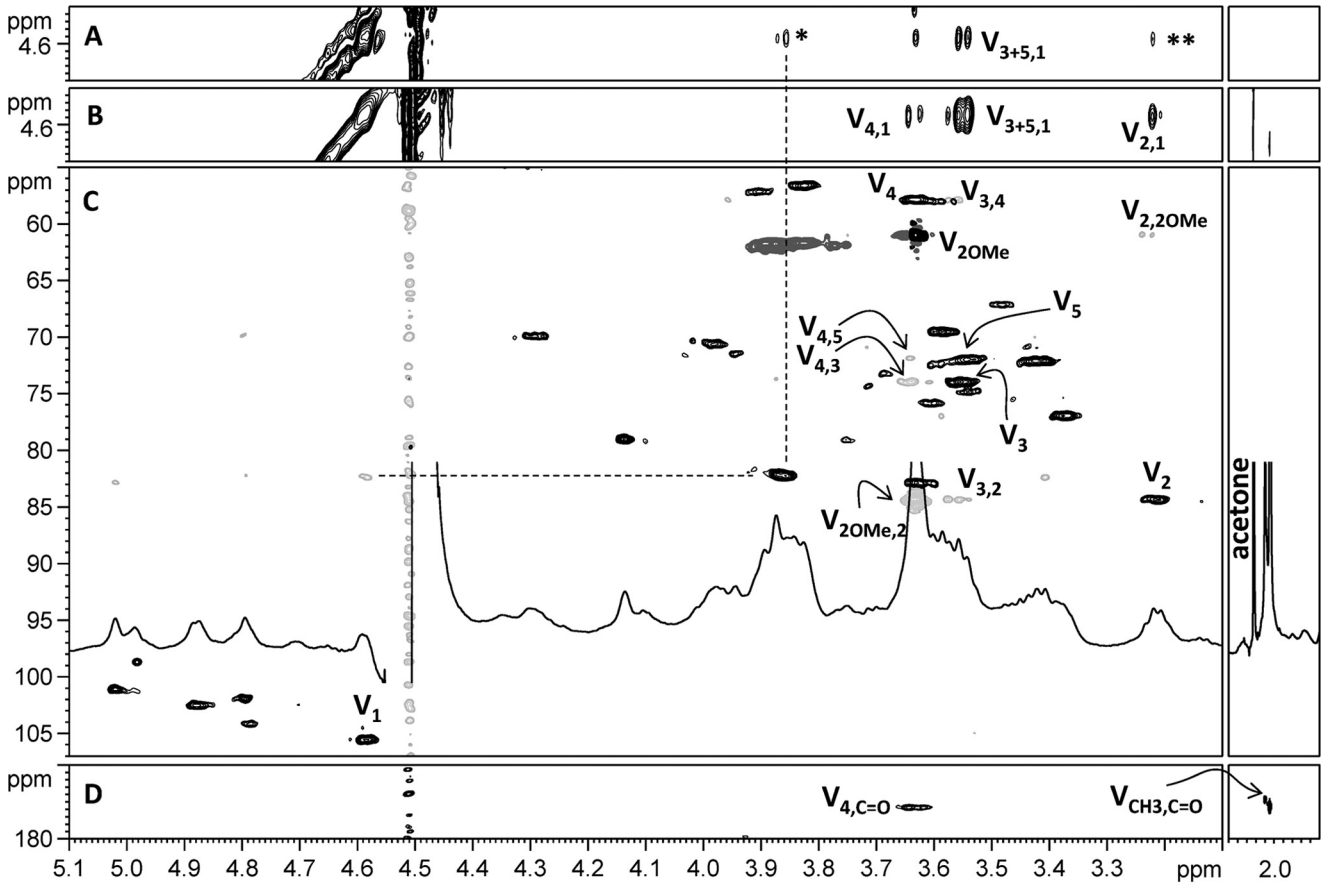

Figure 8. NMR of crude polysaccharide from Mimivirus fibrils. Shown are 2D spectra recorded for the crude polysaccharide from Mimivirus fibrils (600 MHz, 56 °C, D_2O). *A*, expansion of NOESY spectrum showing correlation from Vio (*V*) anomeric proton. *B*, expansion of TOCSY spectrum showing correlation from Vio anomeric proton. *C*, overlap of HSQC (*black*/*dark gray*) and HMBC (*pale gray*) spectra. *D*, expansion of HMBC spectrum detailing the long-range correlations with the carbonyl group. Vio densities are labeled with *V*, and *dotted lines* point to the HSQC density of the residue that has Vio linked. *, inter-residual NOE density between Vio and the other monosaccharide; **, NOESY artifact caused by minimal spin diffusion.

Table 2

^{1}H and ^{13}C chemical shifts of UDP-α-VioNAc as UDP precursor and in the polysaccharide

Spectra calibration used the methyl group of acetone (^{1}H/^{13}C 2.225/31.45 ppm) added as internal standard.

	Nucleus	1	2	3	4	5	6
UDP-VioNAc							
VioNAc	^{1}H	5.57	3.61	3.76	3.62	4.04	1.18
	^{13}C	96.4	73.3	71.8	57.6	69.3	18.2
Ac	^{1}H		2.03				
	^{13}C	175.6	23.3				
Ribose	^{1}H	5.99	4.38	4.37	4.29	4.24–4.20	
	^{13}C	89.5	74.9	70.8	84.5	66.2	
Uracil	^{1}H					5.97	7.96
	^{13}C		152.9		167.5	103.7	142.7
VioNAc (polysaccharide)							
β-VioNAc	^{1}H	4.59	3.22	3.56	3.64	3.54	1.24
	^{13}C	105.3	84.3	73.9	57.8	72.0	18.3
OMe	^{1}H	3.63					
	^{13}C	60.9					
Ac	^{1}H		2.07				
	^{13}C	175.1	23.5				

PerB belongs to class I, because they use a conserved histidine in the active site as a catalytic base. On the other hand, for class II enzymes, comprising QdtC and AntD, a substrate-assisted catalytic mechanism has been proposed (36). To confirm that N-L142 also belongs to class I acetyltransferases, we have performed site-directed mutagenesis of the proposed catalytic His residue. Indeed, the H136A mutant activity, assayed immediately after purification, was 3 orders of magnitude lower when compared with the WT. This finding matches what is described for PglB and PglD His mutants, although the decrease of the catalytic efficiency of these other enzymes ranged from 4 to 6 orders of magnitude. Upon storage, the N-L142 H136A mutant activity decreased faster than the WT, being 70–80% of the original value after 1 week of storage. On the other hand, protein aggregation or precipitation could not be detected, suggesting that His-136 has a minor role in perturbing the struc-

ture of the protein. Accordingly, our data and the comparison of the N-L142 structural model with the published homologous structures clearly pinpointed a catalytic role for this His, as well as the other molecular determinants responsible for substrate specificity.

The C-terminal part of the L142 protein displays a glycosyltrasferase GT-2 fold, suggesting that this domain can be responsible for the attachment of the acetylated Vio on the Mimivirus fibers. Interestingly, NMR analysis has revealed that VioNAc is bound via a β-anomeric linkage, thus indicating that the involved enzyme behaves as an inverting transferase. Several GT-2 enzymes are contained in the same gene cluster as L142 and are probably derived from gene duplication and fusion events. The origin of this cluster is not clear, because it contains genes related to both prokaryotes (*i.e.* L136 and L142) and eukaryotes (R141). However, because these putative GTs are only found in Mimiviridae members of group A, it is likely that they are involved in the transfer of the monosaccharides that are uniquely produced by these viruses, *i.e.* rhamnose and Vio (6, 7).

The mechanisms of production of the complex carbohydrates of Mimivirus and other large DNA viruses are largely unknown. In addition to *Chlorella* viruses, which revealed the presence of novel and unique structures (3), glycans from other viral families still await characterization. Several evidences have already suggested that glycosylation occurs in the cytosol, in the so-called "viral factories," but information about the organization of the glycosylation machinery in these factories is still lacking, as well as on the origin of the enzymes involved in these processes. Identification and characterization of the enzymes encoded by the viral genomes will help shed light on these issues.

Experimental procedures

L142 sequence and structural analyses

The most similar homologues of the N- and C-terminal domains of L142 were identified using the BLAST tool on the NCBI server, using the "nr" and the "env-nr" databases. The CAZy database was also used for glycosyltransferase identification (29). The N-L142 sequence was submitted to the Phyre server (37), which returned a model of the L142 N-terminal domain (Leu-8 to Ile-206) based on the PglB structure from *N. gonorrhoeae* (100% confidence, 4M99) (32). We used the 4M99 structure to model the acetyl-CoA cofactor in the N-terminal domain of the L142 binding site and the PerB structure in complex with acetyl-CoA and GDP-D-*N*-acetylperosamine (4EA8) to define the nucleotide acetylated sugar-binding site (34). A model of UDP-D-VioNAc manually built from the GDP-D-N-acetylperosamine and UDP-D-BacNAc$_2$ (3BSS, 31) was fitted in the nucleotide sugar-binding pocket of N-L142. We used the molecular visualization program VMD (38) to compare the four structures (PglB, PerB, PglD, and WeeI) and define the amino acids involved in ligand binding.

Expression and purification of recombinant L142 proteins

The N-L142 (amino acids 1–213) was expressed as a recombinant GST-fusion protein in *E. coli* strain BL21 (DE3) (New England Biolabs) using the pGEX-6-P1 vector (GE Healthcare). The PCR-amplified sequence corresponding to bases 1–639 of *L142* ORF was digested with BamHI-HF® and XhoI restriction enzymes (New England Biolabs) and ligated in the plasmid vector. Site-directed mutagenesis was performed using QuikChange (Agilent), following the recommended protocols. Primers were designed using QuikChange primer design program. Sequencing of WT and mutants was performed by TibMolbiol (Genova, Italy). Protein expression, purification, and proteolytic cleavage were performed as described previously (8). Proteins were concentrated to ~1 mg/ml using Amicon Ultra-4 10K (Millipore) and stored in PBS at 4 °C. They were analyzed by UV absorbance from 210 to 340 nm, and concentration was determined using ϵ_{280} = 15,930 M^{-1} cm^{-1} (39). Purity was determined by SDS-PAGE.

Enzymatic assays

Mimivirus N-L142 enzymatic activity was assayed on the UDP-D-Vio, produced using recombinant Mimivirus R141 and L136 (6, 8). UDP-D-Vio was incubated with acetyl-CoA in presence of N-L142 in PBS, pH 7.3, at 25 °C. Reactions with different concentrations of substrates were performed. The reactions were stopped by heat inactivation for 3 min at 80 °C at different time points of incubation, and the solutions were clarified by microfiltration (Millipore). After clarification, the reaction mixtures were analyzed by HPLC, as previously described (7). Specific activity was determined using the reduction of UDP-D-Vio peak area and expressed as means ± S.D. of μmol converted per min/mg protein, using 0.2 mM UDP-D-Vio and 0.4 mM acetyl-CoA as substrates. Analyses were performed in duplicate at different time points after enzyme purification from two independent protein preparations.

Structural characterization of L142 product

To confirm the acyltransferase activity of Mimivirus N-L142, its product was purified as previously described (6) and analyzed by ESI-MS and by NMR. ESI-MS analysis was performed in direct infusion analysis at 5 μl/min on an Agilent 1100 series LC/MSD ion trap XCT instrument (Agilent Technologies, Palo Alto, CA). Nucleotide sugars were diluted up to 10 pmol/ml in a water:acetonitrile (50:50) solution containing 0.1% formic acid. The spectra were acquired in negative ion mode in the mass range of the expected m/z ratios, as described (6).

For NMR analysis, 1D and 2D NMR spectra were recorded on a Bruker 600 DRX equipped with a CryoProbe™ on a solution of 500 μl of D_2O, at 25 °C. Double quantum filtered phase-sensitive homonuclear COSY experiment was performed using data sets of 2048 × 512 points (40, 41); the data matrix was zero-filled in both dimensions to give a matrix of 4K × 2K points and was resolution-enhanced in both dimensions by a cosine-bell function before Fourier transformation. Coupling constants were determined on a first order basis from high-resolution 1D spectra. HSQC and HMBC spectra were measured in the ^{1}H-detected mode via single quantum coherence with proton decoupling in the ^{13}C domain, using data sets of 2048 × 512 points. Experiments were carried out in the phase-sensitive mode (40), and the data matrix was extended to 4096 × 2048 points using forward linear prediction extrapolation.

Analysis of VioNAc presence on Mimivirus glycan

The presence of acylation on the C-4 amino group of Vio in Mimivirus glycans was verified using the PMAA derivatization technique (42). Approximately 0.5–1 $\times$ 10^{11} whole Mimivirus particles were lyophilized overnight to remove any trace of water that could inhibit the following permethylation reaction. The dry viral particles were suspended in DMSO (1 ml) with powdered NaOH. Then methyl iodide (0.5 ml) was added, and the sample was stirred for 45 min at room temperature. The reaction was quenched by dropwise addition of 5% acetic acid aqueous solution. To purify the permethylated particles, 2 ml of chloroform was added, and the reaction mixture was made up to 5 ml with ultrapure water. The sample was thoroughly mixed and allowed to settle into two layers. The upper aqueous layer was removed and discarded. The chloroform layer was washed several times with ultrapure water and dried under a gentle stream of nitrogen.

The dry permethylated particles were hydrolyzed with TFA and further processed to obtain the alditol acetate derivatives, as previously described (7). The PMAA were extracted from the solid crust at the bottom of the vial four times with 0.5 ml of dichloromethane and collected in a new vial. The samples, evaporated and suspended in a small volume of dichloromethane, were analyzed by GC-MS as previously described (7).

Isolation of Mimivirus polysaccharides and NMR analysis

Mimivirus suspension (2 ml, $\sim$ 2.4 $\times$ 10^{11} particles) were stirred with 6 ml of 0.5 M DTT solution at 100 °C for 1 h to promote the complete removal of the fibrils. The slurry was centrifuged (8000 rpm, 10 min), and the solid was washed twice with ultrapure water. Supernatants were pooled and dialyzed, yielding to a crude polysaccharide preparation (32 mg), and an aliquot (5 mg) was analyzed *via* NMR without further purification. NMR conditions were the same as described for UDP-D-VioNAc, except temperature that was set to 56 °C, and TOCSY and NOESY spectra were recorded, by using 100- and 200-ms mixing time, respectively. The spectra were calibrated using the methyl group of acetone ($^{1}H/^{13}C$ 2.225/31.45 ppm) added as internal standard.

Author contributions—F. P., M. G., and M. E. L. performed protein cloning and expression, mutagenesis, enzyme analysis, sample preparation, and purification for further characterization. F. P. and C. A. performed bioinformatic analyses. A. S. and G. D. analyzed samples by ESI-MS and GC-MS. C. D. C. and A. N. performed NMR analysis. C. A. and S. J. developed and analyzed the L142 structural model. M. G. T. conceived and coordinated the study and wrote the paper. All authors analyzed the results and approved the final version of the manuscript.

References

1. Piacente, F., Gaglianone, M., Laugieri, M. E., and Tonetti, M. G. (2015) The autonomous glycosylation of large DNA viruses. *Int. J. Mol. Sci.* **16,** 29315–29328
2. Van Etten, J. L., Gurnon, J. R., Yanai-Balser, G. M., Dunigan, D. D., and Graves, M. V. (2010) *Chlorella* viruses encode most, if not all, of the machinery to glycosylate their glycoproteins independent of the endoplasmic reticulum and Golgi. *Biochim. Biophys. Acta* **1800,** 152–159
3. De Castro, C., Molinaro, A., Piacente, F., Gurnon, J. R., Sturiale, L., Palmigiano, A., Lanzetta, R., Parrilli, M., Garozzo, D., Tonetti, M. G., and Van Etten, J. L. (2013) Structure of *N*-linked oligosaccharides attached to chlorovirus PBCV-1 major capsid protein reveals unusual class of complex *N*-glycans. *Proc. Natl. Acad. Sci. U.S.A.* **110,** 13956–13960
4. De Castro, C., Speciale, I., Duncan, G., Dunigan, D. D., Agarkova, I., Lanzetta, R., Sturiale, L., Palmigiano, A., Garozzo, D., Molinaro, A., Tonetti, M., and Van Etten, J. L. (2016) *N*-Linked glycans of chloroviruses sharing a core architecture without precedent. *Angew. Chem. Int. Ed. Engl.* **55,** 654–658
5. Hülsmeier, A. J., and Hennet, T. (2014) *O*-Linked glycosylation in *Acanthamoeba polyphaga* Mimivirus. *Glycobiology* **24,** 703–714
6. Piacente, F., Marin, M., Molinaro, A., De Castro, C., Seltzer, V., Salis, A., Damonte, G., Bernardi, C., Claverie, J. M., Abergel, C., and Tonetti, M. (2012) Giant DNA virus Mimivirus encodes pathway for biosynthesis of unusual sugar 4-amino-4,6-dideoxy-D-glucose (Viosamine). *J. Biol. Chem.* **287,** 3009–3018
7. Piacente, F., De Castro, C., Jeudy, S., Molinaro, A., Salis, A., Damonte, G., Bernardi, C., Abergel, C., and Tonetti, M. G. (2014) Giant virus megavirus chilensis encodes the biosynthetic pathway for uncommon acetamido sugars. *J. Biol. Chem.* **289,** 24428–24439
8. Parakkottil Chothi, M., Duncan, G. A., Armirotti, A., Abergel, C., Gurnon, J. R., Van Etten, J. L., Bernardi, C., Damonte, G., and Tonetti, M. (2010) Identification of an L-rhamnose synthetic pathway in two nucleocytoplasmic large DNA viruses. *J. Virol.* **84,** 8829–8838
9. Piacente, F., Bernardi, C., Marin, M., Blanc, G., Abergel, C., and Tonetti, M. G. (2014) Characterization of a UDP-*N*-acetylglucosamine biosynthetic pathway encoded by the giant DNA virus Mimivirus. *Glycobiology* **24,** 51–61
10. Luther, K. B., Hülsmeier, A. J., Schegg, B., Deuber, S. A., Raoult, D., and Hennet, T. (2011) Mimivirus collagen is modified by bifunctional lysyl hydroxylase and glycosyltransferase enzyme. *J. Biol. Chem.* **286,** 43701–43709
11. Rommel, A. J., Hülsmeier, A. J., Jurt, S., and Hennet, T. (2016) Giant Mimivirus R707 encodes a glycogenin paralog polymerizing glucose through α- and β-glycosidic linkages. *Biochem. J.* **473,** 3451–3462
12. Iyer, L. M., Balaji, S., Koonin, E. V., and Aravind, L. (2006) Evolutionary genomics of nucleo-cytoplasmic large DNA viruses. *Virus Res.* **117,** 156–184
13. Raoult, D., Audic, S., Robert, C., Abergel, C., Renesto, P., Ogata, H., La Scola, B., Suzan, M., and Claverie, J. M. (2004) The 1.2-megabase genome sequence of Mimivirus. *Science* **306,** 1344–1350
14. Legendre, M., Santini, S., Rico, A., Abergel, C., and Claverie, J. M. (2011) Breaking the 1000-gene barrier for Mimivirus using ultra-deep genome and transcriptome sequencing. *Virol. J.* **8,** 99
15. Yamamoto, M., Ohnishi-Kameyama, M., Nguyen, C. L., Taguchi, F., Chiku, K., Ishii, T., Ono, H., Yoshida, M., and Ichinose, Y. (2011) Identification of genes involved in the glycosylation of modified viosamine of flagellins in *Pseudomonas syringae* by mass spectrometry. *Genes* **2,** 788–803
16. Taguchi, F., Yamamoto, M., Ohnishi-Kameyama, M., Iwaki, M., Yoshida, M., Ishii, T., Konishi, T., and Ichinose, Y. (2010) Defects in flagellin glycosylation affect the virulence of *Pseudomonas syringae* pv. *tabaci* 6605. *Microbiology* **156,** 72–80
17. Dong, S., McPherson, S. A., Wang, Y., Li, M., Wang, P., Turnbough, C. L., Jr., and Pritchard, D. G. (2010) Characterization of the enzymes encoded by the anthrose biosynthetic operon of *Bacillus anthracis*. *J. Bacteriol.* **192,** 5053–5062
18. Arbatsky, N. P., Kondakova, A. N., Shashkov, A. S., Drutskaya, M. S., Belousov, P. V., Nedospasov, S. A., Petrova, M. A., and Knirel, Y. A. (2010) Structure of the O-antigen of *Acinetobacter lwoffii* EK30A: identification of d-homoserine, a novel non-sugar component of bacterial polysaccharides. *Org. Biomol. Chem.* **8,** 3571–3577
19. Kondakova, A. N., Linder, B., Fudala, R., Senchenkova, S. N., Moll, H., Shashkov, A. S., Kaca, W., Zähringer, U., and Knirel, Y. A. (2004) New structures of the O-specific polysaccharides of proteus: 4. polysaccharides containing unusual acidic *N*-acyl derivatives of 4-amino-4,6-dideoxy-D-glucose. *Biochemistry* **69,** 1034–1043

20. Liu, B., Chen, M., Perepelov, A. V., Liu, J., Ovchinnikova, O. G., Zhou, D., Feng, L., Rozalski, A., Knirel, Y. A., and Wang, L. (2012) Genetic analysis of the O-antigen of *Providencia alcalifaciens* O30 and biochemical characterization of a formyltransferase involved in the synthesis of a Qui4N derivative. *Glycobiology* **22,** 1236–1244
21. Perepelov, A. V., Wang, Q., Senchenkova, S. N., Shevelev, S. D., Shashkov, A. S., Feng, L., Knirel, Y. A., and Wang, L. (2008) Structure and characterization of the gene cluster of the O-antigen of *Escherichia coli* O49 containing 4,6-dideoxy-4-[(*S*)-3-hydroxybutanoylamino]-D- glucose. *Biochemistry* **73,** 406–410
22. Wang, Y., Xu, Y., Perepelov, A. V., Qi, Y., Knirel, Y. A., Wang, L., and Feng, L. (2007) Biochemical characterization of dTDP-D-Qui4N and dTDP-D-Qui4NAc biosynthetic pathways in *Shigella dysenteriae* type 7 and *Escherichia coli* O7. *J. Bacteriol.* **189,** 8626–8635
23. Ovchinnikova, O. G., Valueva, O. A., Kocharova, N. A., Arbatsky, N. P., Maszewska, A., Zablotni, A., Shashkov, A. S., Rozalski, A., and Knirel, Y. A. (2013) Structure of the *O*-polysaccharide of *Providencia alcalifaciens* O35 containing an N-[(S)-1-carboxyethyl]-L-alanine (alanopine) derivative of 4-amino-4,6-dideoxyglucose. *Carbohydr. Res.* **375,** 73–78
24. Kondakova, A. N., Kirsheva, N. A., Shashkov, A. S., Shaikhutdinova, R. Z., Arabtsky, N. P., Ivanov, S. A., Anisimov, A. P., and Knirel, Y. A. (2011) Low structural diversity of the O-polysaccharides of *Photorhabdus asymbiotica* subspp. *asymbiotica* and *australis* and their similarity to the *O*-polysaccharides of taxonomically remote bacteria including *Francisella tularensis*. *Carbohydr. Res.* **346,** 1951–1955
25. Vinogradov, E., Nossova, L., Korenevsky, A., and Beveridge, T. J. (2005) The structure of the capsular polysaccharide of *Shewanella oneidensis* strain MR-4. *Carbohydr. Res.* **340,** 1750–1753
26. Boyer, M., Azza, S., Barrassi, L., Klose, T., Campocasso, A., Pagnier, I., Fournous, G., Borg, A., Robert, C., Zhang, X., Desnues, C., Henrissat, B., Rossmann, M. G., La Scola, B., and Raoult, D. (2011) Mimivirus shows dramatic genome reduction after intraamoebal culture. *Proc. Natl. Acad. Sci. U.S.A.* **108,** 10296–10301
27. Klose, T., Herbst, D. A., Zhu, H., Max, J. P., Kenttämaa, H. I., and Rossmann, M. G. (2015) A Mimivirus enzyme that participates in viral entry. *Structure* **23,** 1058–1065
28. Lombard, V., Golaconda Ramulu, H., Drula, E., Coutinho, P. M., and Henrissat, B. (2014) The carbohydrate-active enzymes database (CAZy) in 2013. *Nucleic Acids Res.* **42,** D490–D495
29. Raetz, C. R., and Roderick, S. L. (1995) A left-handed parallel β helix in the structure of UDP-*N*-acetylglucosamine acyltransferase. *Science* **270,** 997–1000
30. Kubiak, R. L., and Holden, H. M. (2012) Structural studies of AntD: an *N*-acyltransferase involved in the biosynthesis of D-anthrose. *Biochemistry* **51,** 867–878
31. Thoden, J. B., Cook, P. D., Schäffer, C., Messner, P., and Holden, H. M. (2009) Structural and functional studies of QdtC: an *N*-acetyltransferase required for the biosynthesis of dTDP-3-acetamido-3,6-dideoxy-α-D-glucose. *Biochemistry* **48,** 2699–2709
32. Morrison, M. J., and Imperiali, B. (2013) Biochemical analysis and structure determination of bacterial acetyltransferases responsible for the biosynthesis of UDP-*N*,*N*′-diacetylbacillosamine. *J. Biol. Chem.* **288,** 32248–32260
33. Olivier, N. B., and Imperiali, B. (2008) Crystal structure and catalytic mechanism of PglD from *Campylobacter jejuni*. *J. Biol. Chem.* **283,** 27937–27946
34. Thoden, J. B., Reinhardt, L. A., Cook, P. D., Menden, P., Cleland, W. W., and Holden, H. M. (2012) Catalytic mechanism of perosamine *N*-acetyltransferase revealed by high-resolution X-ray crystallographic studies and kinetic analyses. *Biochemistry* **51,** 3433–3444
35. Arora, S. K., Bangera, M., Lory, S., and Ramphal, R. (2001) A genomic island in *Pseudomonas aeruginosa* carries the determinants of flagellin glycosylation. *Proc. Natl. Acad. Sci. U.S.A.* **98,** 9342–9347
36. Chantigian, D. P., Thoden, J. B., and Holden, H. M. (2013) Structural and biochemical characterization of a bifunctional ketoisomerase/*N*-acetyltransferase from *Shewanella denitrificans*. *Biochemistry* **52,** 8374–8385
37. Kelley, L. A., Mezulis, S., Yates, C. M., Wass, M. N., and Sternberg, M. J. (2015) The Phyre2 web portal for protein modeling, prediction and analysis. *Nat. Protoc.* **10,** 845–858
38. Humphrey, W., Dalke, A., and Schulten, K. (1996) VMD: visual molecular dynamics. *J. Mol. Graph.* **14,** 33–38, 27–28
39. Gasteiger, E. H., Gattiker. A., Duvaud, S., Wilkins, M. R., Appel, R. D., and Bairoch A;. (2005) Protein Identification and Analysis Tools on the ExPASy server. In *The Proteomics Protocols Handbook* (Walker, J. M., ed) pp. 571–607, Humana Press, Totowa, NJ
40. States, D. J., Haberkorn, R. A., and Ruben, D. J. (1982) A two-dimensional nuclear Overhauser experiment with pure absorption phase in four quadrants. *J. Magn. Reson.* **48,** 286
41. Rance, M., Sørensen, O. W., Bodenhausen, G., Wagner, G., Ernst, R. R., and Wüthrich, K. (1983) Improved spectral resolution in COSY ^{1}H NMR spectra of proteins via double quantum filtering. *Biochem. Biophys. Res. Commun.* **117,** 479–485
42. Ciucanu, I. (2006) Per-*O*-methylation reaction for structural analysis of carbohydrates by mass spectrometry. *Anal. Chim. Acta* **576,** 147–155
43. Marchler-Bauer, A., Derbyshire, M. K., Gonzales, N. R., Lu, S., Chitsaz, F., Geer, L. Y., Geer, R. C., He, J., Gwadz, M., Hurwitz, D. I., Lanczycki, C. J., Lu, F., Marchler, G. H., Song, J. S., Thanki, N., *et al.* (2015) CDD: NCBI's conserved domain database. *Nucleic Acids Res.* **43,** 222–226

The rare sugar *N*-acetylated viosamine is a major component of Mimivirus fibers

Francesco Piacente, Cristina De Castro, Sandra Jeudy, Matteo Gaglianone, Maria Elena Laugieri, Anna Notaro, Annalisa Salis, Gianluca Damonte, Chantal Abergel and Michela G. Tonetti

J. Biol. Chem. 2017, 292:7385-7394.
doi: 10.1074/jbc.M117.783217 originally published online March 17, 2017